WATER RESOURCES RESEARCH, VOL. 49, 1–13, doi:10.1002/wrcr.20313, 2013

Trapping and hysteresis in two-phase flow in porous media: A pore-network study

V. Joekar-Niasar,[1] F. Doster,[2,3] R. T. Armstrong,[4] D. Wildenschild,[4] and M. A. Celia[2]

Received 18 July 2012; revised 25 April 2013; accepted 15 May 2013.

[1] Several models for two-phase flow in porous media identify trapping and connectivity of fluids as an important contribution to macroscale hysteresis. This is especially true for hysteresis in relative permeabilities. The trapping models propose trajectories from the initial saturation to the end saturation in various ways and are often based on experiments or pore-network model results for the endpoints. However, experimental data or pore-scale model results are often not available for the trajectories, that is, the fate of the connectivity of the fluids while saturation changes. Here, using a quasi static pore-network model, supported by a set of pore-scale laboratory experiments, we study how the topology of the fluids changes during drainage and imbibition including first, main and scanning curves. We find a strong hysteretic behavior in the relationship between disconnected nonwetting fluid saturation and the wetting fluid saturation in a water-wet medium. The coalescence of the invading nonwetting phase with the existing disconnected nonwetting phase depends critically on the presence (or lack thereof) of connected nonwetting phase at the beginning of the drainage process as well as on the pore geometry. This dependence involves a mechanism we refer to as "reversible corner filling." This mechanism can also be seen in laboratory experiments in volcanic tuff. The impact of these pore-network model results on existing macroscopic models is discussed.

Citation: Joekar-Niasar, V., F. Doster, R. T. Armstrong, D. Wildenschild, and M. A. Celia (2013), Trapping and hysteresis in two-phase flow in porous media: A pore-network study, *Water Resour. Res.*, *49*, doi:10.1002/wrcr.20313.

1. Introduction

[2] Two-phase flow in porous media is important in many scientific fields, including hydrology, petroleum reservoir engineering, and soil science. Standard approaches to model two-phase flow involve mass balance equations for the fluids or components in the system, some version of Darcy's law modified to account for the presence of multiple fluid phases, and a relationship between capillary pressure and phase saturation. The modifier in the Darcy equation is the relative permeability function, which is usually taken to be a nonlinear function of phase saturation. The capillary pressure is also usually taken to be a nonlinear function of saturation. Both of these nonlinear functions contain residual phase saturations and exhibit hysteresis, two characteristics of multiphase porous media systems that are often important in practical problems.

[3] Residual saturation of one phase, call it phase *n*, is a result of the development of subregions of phase *n* that become hydraulically isolated within the pores, such that each isolated region of fluid *n* is surrounded by the other fluid phase, call it fluid *w*. Isolated region of fluid *n* loses connection with the bulk (or connected) portion of that fluid (*n*) (see Figure 1). The amount of isolated fluid, which under most conditions is considered to be immobile and trapped, is important for many applications, including oil reservoir analysis where trapped oil (or gas) means less production of hydrocarbon, and carbon sequestration problems where trapping of CO_2 leads to safe underground storage.

[4] Hysteresis refers to a process- and history-dependent relationship. This process dependence is a result of the complex geometry and topology of the interconnected pore space in porous materials as well as the hysteresis of contact angle. The effect of pore geometry on hysteresis in capillary pressure and relative permeability curves has been investigated extensively using a pore-network model by *Jerauld and Salter* [1990]. However, Jerauld and Salter only marginally addressed how the disconnected nonwetting phase evolves and how it depends on the fluid topology.

[5] A number of mathematical models to describe various aspects of hysteretic functions have been proposed in the literature. Two general approaches have evolved. The first is based on the concept that drainage (invasion by a nonwetting fluid, *n*) tends to follow a different pattern than imbibition (invasion by a wetting fluid, *w*). This concept argues that regions of the pore space domain are accessed differently during drainage and imbibition. A classic example of this type of approach is that of *Mualem* [1974]; related work includes *Parker and Lenhard* [1987] and *Scott et al*. [1983]. A second approach is based on the idea that

[1]Department of Earth Sciences, Utrecht University, Utrecht, Netherlands.
[2]Department of Civil and Environmental Engineering, Princeton University, Princeton, New Jersey, USA.
[3]Department of Mathematics, Bergen University, Bergen, Norway.
[4]School of Chemical, Biological and Environmental Engineering, Oregon State University, Oregon, USA.

Corresponding author: V. Joekar-Niasar, Department of Earth Sciences, Utrecht University, Utrecht, NL-3508 TA, Netherlands. (vjoekar@gmail.com)

0043-1397/13/10.1002/wrcr.20313

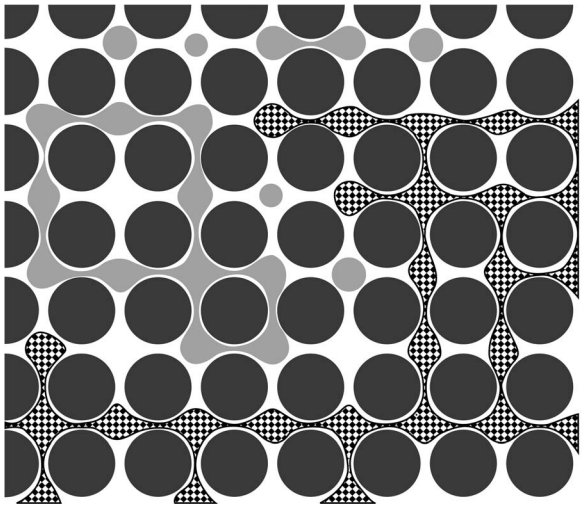

Figure 1. Conceptual picture of the connected (checkboard) and nonconnected (light gray) nonwetting fluid phase. The wetting fluid is depicted white and the porous medium by dark gray spheres.

hysteresis is due to an insufficient or incomplete description of the system, and additional internal state variables need to be included in the description. This idea dates at least to *Everett and Whitton* [1952], with recent examples including theories that suggest interfacial area as an additional variable [*Hassanizadeh and Gray*, 1993; *Niessner and Hassanizadeh*, 2008] as well as theories suggesting that the phases should be further refined into connected and disconnected regions [*Hilfer*, 2006; *Doster et al*., 2010]. Other models focused on trapping have also been proposed, beginning with the classic work of *Land* [1968], who looked at the amount of nonwetting phase trapped after an incomplete first-drainage cycle (that is, drainage from full saturation of wetting phase to some intermediate saturation, called the turning-point saturation) followed by imbibition. Land related the trapped (or residual) saturation at the end of the imbibition to the turning-point saturation. Other notable models that have focused on nonwetting-phase trapping include *Jerauld* [1997], *van Kats and van Duijn* [2001], *Land* [1968], and *Spiteri et al*. [2005].

[6] One interesting aspect of fluid trapping is how the topology of trapped regions develops and evolves as the fluid saturation changes, for example, from the turning-point saturation described earlier, where there is no trapped fluid, to the saturation at the end of the imbibition cycle, where there may be significant amounts of trapped fluid. We may also reasonably ask, given the hysteretic nature of the major constitutive relationships such as capillary pressure and relative permeability curves, whether or not the relationship between trapped fluid and phase saturation is itself hysteretic. Because trapped regions are difficult to observe in typical physical experiments, and because they appear to play significant roles in many problems of practical interest, we will use computational tools that allow us to track explicitly fluid configurations on the pore scale and thereby identify trapped fluid regions as they form. Our tool of choice is a pore-scale network model described in *Joekar-Niasar and Hassanizadeh* [2011]. This model uses a network of pore bodies and pore throats with different choices for the geometry of the pore elements. With these models, we can simulate invasion experiments under a wide variety of conditions, impose multiple turning points in both drainage and imbibition, simulate many cycles of drainage and imbibition with arbitrary stopping points, and impose different kinds of boundary conditions.

[7] In this study we present

[8] The evolution of trapping, with specific focus on the general functional form of the trapping function (trapped nonwetting phase saturation versus the wetting phase saturation) and whether or not it exhibits hysteresis.

[9] The qualitative differences among the different models proposed in the literature for trapping. We also examine how trapping relates to hysteresis in the standard capillary pressure and relative permeability functions.

[10] A new phenomenon in the trapping relationship from the pore-network model, which we corroborate with recent novel experimental data. This phenomenon, referred to as "reversible corner filling," can cause different trajectory trends of trapped saturation depending on pore geometry and initial nonwetting-phase fluid topology. This has not been addressed before in the literature.

[11] The paper is structured as follows. In section 2, we provide a survey of existing trapping models, beginning with the classic model of *Land* [1968]. In section 3, we provide an overview of the salient features of the pore-scale network model that we use in the study. In section 4, we describe the computational experiments that are performed and report results related to both trapping and overall hysteresis, including the associated capillary pressure and relative permeability functions. The results are compared, qualitatively, to results from experiments performed on volcanic tuff material. Finally, in section 5, we present a discussion of the results and a set of conclusions.

2. Continuum-Scale Models

[12] Continuum-scale trapping models for the nonwetting phase consist of two parts. The first part determines the saturation of the remaining nonwetting fluid in the porous medium after a completed imbibition cycle. It is called the residual saturation of the nonwetting phase S_{nr}. In most models, this quantity is assumed to be either a constant or a function of the maximum nonwetting saturation $\left(S_{rn}^{\max}\right)$ which has been reached. That maximum saturation is called the turning-point saturation, S_n^t (refer to Figure 2). The second part of a trapping model determines the saturation of the disconnected (or trapped) nonwetting fluid, S_n^d, for a given wetting fluid saturation, S_w. The connected nonwetting fluid saturation S_n^c sums with the disconnected saturation, S_n^d, to give the total nonwetting saturation $S_n = S_n^c + S_n^d$. Note that for most porous media, the wetting phase also has a residual or irreducible saturation S_{wr}. In this paper, we assume that the residual wetting-phase saturation is a constant. This assumption permits us to rescale the saturations so that $S_w = S_{wr} \rightarrow S_{wr} = 0$.

2.1. Land's Model

[13] In *Land* [1968] both parts of a trapping model are proposed. Based on experimental data, Land deduced that the difference of the reciprocals between the turning-point saturation, S_n^t, and the residual saturation, S_{nr}, is approximately

constant for a given system. Hence, the measurement of one pair, for example, the extreme values $S_n^t = 1$ and $S_{rn}^{\max} = S_{rn}(1)$, suffices to determine the relationship

$$S_{nr}(S_n^t) = \frac{S_n^t}{1 + (1/S_{rn}^{\max} - 1)S_n^t}. \quad (1)$$

[14] Land also postulated that equation (1) will hold for any connected nonwetting saturation S_n^c; therefore the disconnected nonwetting saturation, S_n^d, is the difference between the two residual saturations, $S_{nr}(S_n^t)$ and $S_{nr}(S_n^c)$. In terms of the nonwetting saturation S_n, this leads directly to the following relation,

$$S_n^d(S_n; S_n^t) = \frac{1}{2}\left[(S_n + S_{nr}(S_n^t)) - \sqrt{(S_n - S_{nr}(S_n^t))^2 + \frac{4}{1/S_{rn}^{\max} - 1}(S_n - S_{nr}(S_n^t))}\right]. \quad (2)$$

[15] This model has been obtained for a system of water and gas but it is proposed to hold for other fluid pairs, for example, oil and water, if the porous medium is strongly wetting. Even though the model is constructed for imbibition processes, Land suggested that the difference between drainage and imbibition was expected to be small and equation (2) should hold for drainage processes as well. Figure 3a illustrates $S_n^d(S_w; S_n^t)$ for $S_{rn}^{\max} = 0.2$ and $S_n^t = \{1, 0.8, 0.6, 0.3\}$.

2.2. Parker and Lenhard's Model

[16] A simplified version of the Land model was proposed by *Parker et al.* [1987] and *Lenhard and Parker* [1987] for air and water in soils. The authors used equation (1) and interpolated linearly between turning-point saturation and residual saturation to obtain a relationship between S_n^d and S_n. The model thus is written as

$$S_n^d(S_n; S_n^t) = \begin{cases} \dfrac{S_{nr}(S_n^t)}{S_n^t - S_{nr}(S_n^t)}(S_n^t - S_n), & S_n < S_n^t, \\ 0, & S_n \geq S_n^t. \end{cases} \quad (3)$$

[17] The authors justified this approach by the assumption that all pore classes entrap nonwetting fluid in proportion to their volumes and that compression of entrapped fluids can be disregarded at typical pressures in the vadose zone. Figure 3b illustrates this linear trapping relation in combination with Land's residual saturation–turning-point saturation relationship, equation (1), $S_{rn}^{\max} = 0.2$, and $S_n^t = \{1, 0.8, 0.6, 0.3\}$.

2.3. Jerauld's Model

[18] In *Jerauld* [1997], a modification to Land's equation (1) was proposed. The modification was based on empirical data for mixed-wet reservoirs, which suggest that the residual nonwetting phase saturation is less dependent on the turning-point saturation S_n^t for large turning-point saturations than predicted by the Land model. An additional parameter to take this into account was proposed and equation (1) was altered to read

$$S_{nr}(S_n^t) = \frac{S_n^t}{1 + (1/S_{rn}^{\max} - 1)S_n^{t\,a}}. \quad (4)$$

[19] The parameter a is different for gas and oil and is given as $a = 1 + bS_{rn}^{\max}/(1 - S_{rn}^{\max})$ for gas (with the additional fitting parameter b) and $a = 1/(1 - S_{rn}^{\max})$ for oil. A trapping relation $S_n^d(S_n; S_n^t)$ may be obtained analogously to Land's model. However, an explicit algebraic expression $S_n^d(S_n; S_n^t)$ is not possible unless a is an integer. The corresponding implicit nonlinear algebraic equation can be solved numerically to obtain the curves in Figure 3c, with the parameters $a = 1.2$, $S_{rn}^{\max} = 0.2$, and $S_n^t = \{1, 0.8, 0.6, 0.3\}$. Note that compared to Figure 3a the trapping occurs later along the trajectory and hence the difference between different turning-point saturations is smaller for $S_n^t > S_{rn}^{\max}$. For larger a, a process-independent residual saturation becomes a reasonable approximation for $S_n^t > S_{rn}^{\max}$.

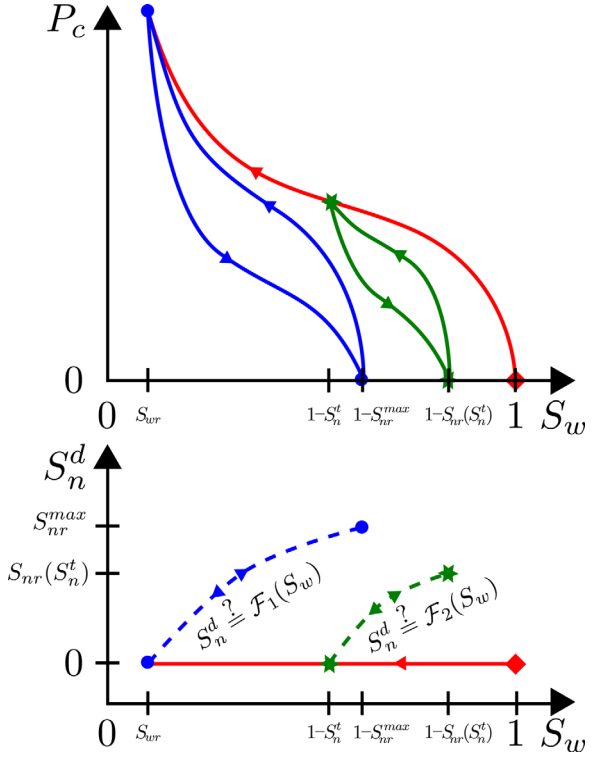

Figure 2. Conceptual picture of hysteresis paths and the link between capillary pressure hysteresis and disconnected nonwetting saturation. Red curves illustrate primary drainage, blue curves the main hysteresis loop, and green curves a hysteresis loop turning at a lower turning-point saturation S_n^t. This article studies the dashed curves with a pore-network model.

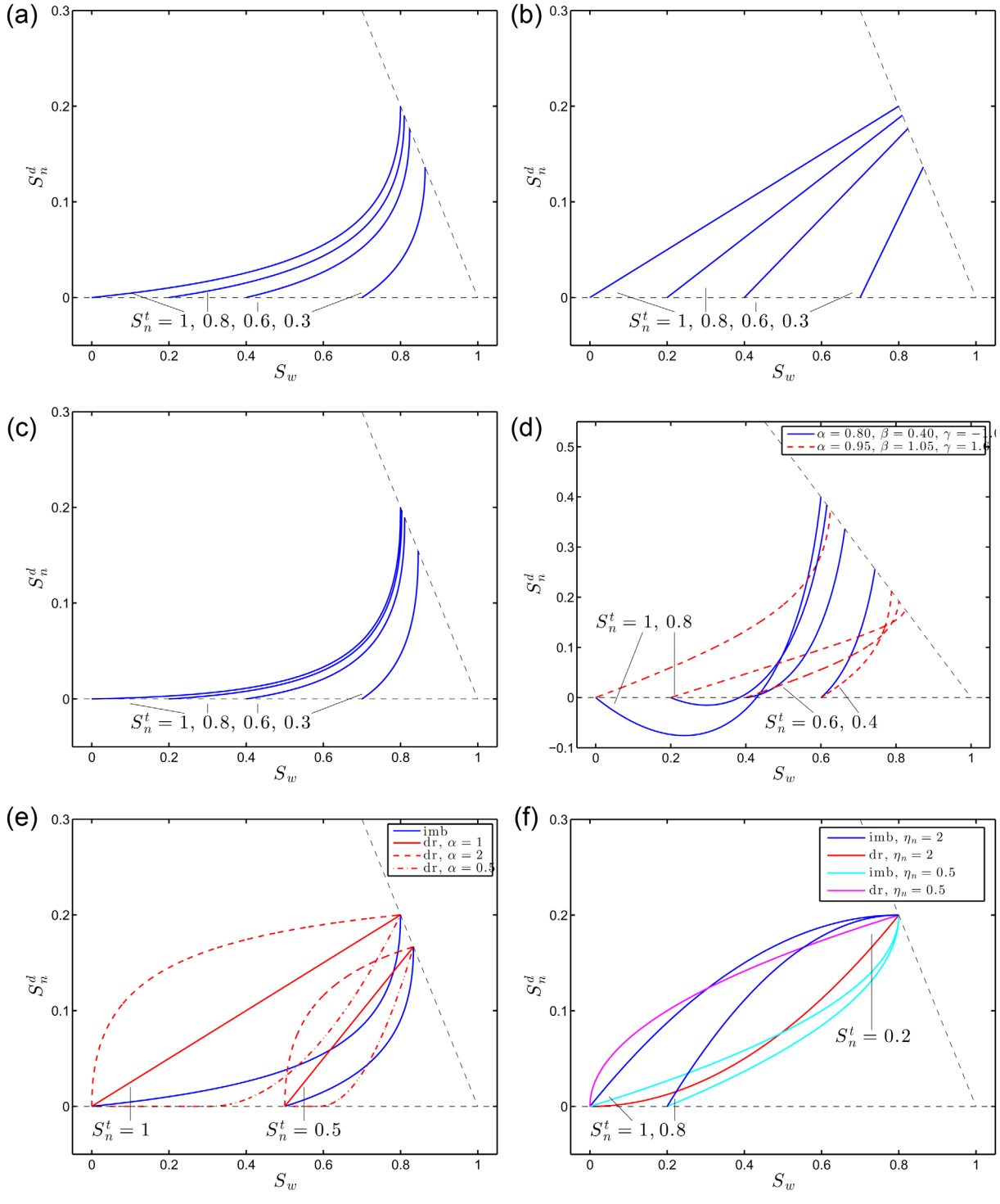

Figure 3. Illustration of the different trapping models: (a) Land, (b) Parker/Lenhard, (c) Jerauld, (d) Spiteri, (e) van Kats, (f) Hilfer. The graphs show the disconnected nonwetting-phase saturation S_n^d with respect to the wetting-phase saturation, $S_w = 1 - S_n$. For all models but the Spiteri model, the traditional residual saturation, that is, the maximum trapped one, is 0.2. The Jerauld parameter in Figure 3c is $a = 1.2$. In Figure 3e and 3f, two parameterizations are shown (see graph for numbers). Note the negative trapped saturations in Figure 3d. In Figure 3e, for each of the two imbibition curves three drainage curves are shown with $\alpha = 1$ (solid), $\alpha = 2$ (dashed), and $\alpha = 0.5$ (dash-dotted).

2.4. Spiteri et al.'s Model

[20] *Spiteri et al.* [2005] proposed a model which differed from Land's approach. The model studies mixed-wet and oil-wet conditions and is based on pore-network model results. Their results show a nonmonotonic behavior for $S_{nr}(S_n^t)$ and the authors use a second-order polynomial,

$$S_{nr}(S_n^t) = \alpha S_n^t - \beta {S_n^t}^2, \tag{5}$$

to fit the numerical results. They also challenge the idea that this equation holds for the connected saturation as well. Instead they subtract a second-order polynomial from the difference weighted with a third parameter. The relation is given by

$$S_n^d(S_n; S_n^t) = S_n - \frac{1}{\beta}\left([\alpha-1] + \left\{[\alpha-1]^2 + 4\left[S_n - S_{nr}(S_n^t) + \gamma\left(S_n - S_{nr}(S_n^t)\right)\left(S_n - S_n^t\right)\right]\right\}^{\frac{1}{2}}\right). \tag{6}$$

[21] The parameters α, β, γ are fitting parameters which have to be determined from experiments. Figure 3d illustrates $S_n^d(S_n; S_n^t)$ for two different parameter sets and for turning-point saturations $S_n^t = \{1, 0.8, 0.6, 0.4\}$. Note that the parameters can be related to the maximum residual saturation as $S_{rn}^{\max} = \alpha - \beta$ for full wetting conditions and main imbibition. The model has to be applied cautiously because the fitting parameters do not represent physical processes and there are parameterizations for which the model predicts unphysical negative disconnected saturations S_n^d even for realistic turning-point saturations S_n^t (see Figure 3d) [see, *Spiteri et al*. 2005].

2.5. van Kats and van Duijn's Model

[22] *van Kats and van Duijn* [2001] proposed a trapping model that, for the first time, takes into account the differences between drainage and imbibition. In this model the process of break up and coalescence is modeled using a set of differential equations. Integration of these differential equations leads to a direct relationship between disconnected and wetting saturation $S_n^d(S_w)$. For imbibition, it is assumed that the production of trapped nonwetting phase, S_n^d, is proportional to the change in apparent water saturation, $S_w^a \equiv S_w + S_n^d$, and that the proportionality factor, f^{im}, is a function of the connected nonwetting phase $f^{\text{im}} = f^{\text{im}}(S_n^c)$. Because of volume conservation, this may be expressed in terms of mobile and trapped nonwetting saturation as follows,

$$\frac{\partial S_n^d}{\partial t} = -f^{\text{im}}(S_n^c)\frac{\partial S_n^c}{\partial t}. \tag{7}$$

[23] The function f^{im} is obtained from Land's trapping relation,

$$f^{\text{im}}(S_n^c; S_{rn}^{\max}) = \frac{1}{\left[1 + \left(1/S_{rn}^{\max} - 1\right)S_n^c\right]^2}. \tag{8}$$

[24] For drainage, it is assumed that the reduction of the disconnected nonwetting phase is proportional to the increase of connected nonwetting phase and that the proportionality factor is a function of the ratio of disconnected nonwetting saturation S_n^d and the volume which is available for nonprimary nonwetting invasion, $S_w^a - S_n^t \equiv 1 - S_n^c - S_n^t$ and hence

$$\frac{\partial S_n^d}{\partial t} = -f^{\text{dr}}(S_n^c, S_n^d)\frac{\partial S_n^c}{\partial t}. \tag{9}$$

[25] Equation (9) holds with

$$f^{\text{dr}}(S_n^c, S_n^d; S_n^t) = \left(\frac{S_n^d}{S_n^c + S_n^t}\right)^{\alpha} \tag{10}$$

and $\alpha > 0$. For $\alpha > 1$ the reduction is mostly happening at the beginning of a drainage while for $\alpha < 1$ the reduction is mostly happening close to S_n^t. The authors take α as a pure fitting parameter and only study the case $\alpha = 1$. Note that the choice $\alpha = 1$ leads to higher residual saturations when switching between drainage and imbibition. In contrast, a small α leads to reduction of residual saturations. Figure 3e illustrates the hysteresis loop for two turning-point saturations $S_n^t = \{1, 0.5\}$ with $S_{rn}^{\max} = 0.2$ and $\alpha = 1$ (solid curves), $\alpha = 0.5$ (dash-dotted curves) and $\alpha = 2$ (dashed curves).

2.6. Hilfer's Model

[26] *Hilfer* [2006] proposed a hysteresis model for two-phase flow in porous media by identifying connected or percolating parts of phases and the complementary disconnected or nonpercolating parts. Each one thus was treated as a different phase.

[27] In several subsequent works [*Doster et al*., 2010; *Doster and Hilfer*. 2011; *Hilfer and Doster*, 2010] the case of immobile disconnected fluid phases was studied, including the specification of a trapping relation for the nonwetting fluid. As in *van Kats and van Duijn* [2001] differences between drainage and imbibition are included and breakup and coalescence were modeled instead of the trapping trajectory. The disconnected nonwetting phase is changed in proportion to the change of total nonwetting phase saturation

$$\frac{\partial S_n^d}{\partial t} = -\eta_n \frac{S_n^d - S_n^{d*}(\partial_t S_n)}{S_n^*(\partial_t S_n) - S_n}\frac{\partial S_n}{\partial t} \tag{11}$$

with a constant parameter η_n, and the process-dependent saturations defined by

$$S_n^{d*} = \begin{cases} \min\left(S_{rn}^{\max}, (1-\epsilon_m)S_n\right), & \partial_t S_n < 0, \\ 0, & \partial_t S_n \geq 0, \end{cases} \qquad S_n^* = \begin{cases} S_n^{d*}, & \partial_t S_n < 0, \\ 1, & \partial_t S_n \geq 0, \end{cases} \tag{12}$$

where ϵ_m is a regularization parameter preventing unphysical saturations. Equation (11) has an algebraic solution given by

$$S_n^d = S_n^{d*} + \left(S_n^{dt} - S_n^{d*}\right)\left(\frac{S_n^* - S_n}{S_n^* - S_n^t}\right)^{\eta_n}, \tag{13}$$

where S_n^{dt} and S_n^t denote the saturations at the last process change. Figure 3f illustrates the trapping relationship for the turning-point saturation pairs $(S_n^t, S_n^{dt}) = \{(1,0), (0.8,0),$

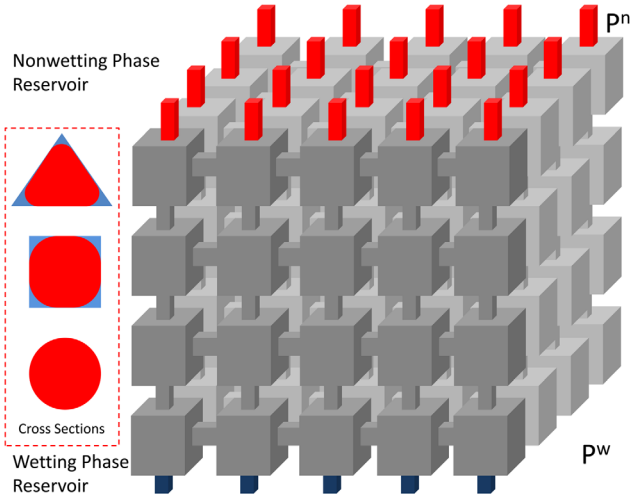

Figure 4. Three-dimensional schematic presentation of the pore network. The inset figures show the cross sections of pore throats.

$(0.2, 0.2)\}$ corresponding to characteristic hysteresis processes for $S_{rn} = 0.2$ and $\eta_n = 2$ (blue and red curves) and $\eta_n = 0.5$ (pink and cyan curves). Two features distinguish this model from those previously discussed. First, the residual saturation S_{nr} changes with the turning-point saturation only for $S_n^t < S_{rn}^{\max}$. Second, the curvature of the trapping relation has a different sign for $\eta_n < 1$ and $\eta_n > 1$. For $\eta_n > 1$ the sign of the curvature of the trapping relation for imbibition is different from the other models.

3. Pore-Network Model

[28] Pore-network models have been used extensively to foster the understanding of phenomena related to porous media flow [*Blunt*, 2001; *Joekar-Niasar and Hassanizadeh*, 2012]. Here, we use a quasi static pore-network model developed by *Joekar-Niasar et al*. [2008, 2010a] to study how trapping of the nonwetting fluid actually evolves. Since in quasi static pore-network models only equilibrium situations under capillary dominated regimes are simulated, the effect of dynamic parameters such as viscosity ratio and capillary number on trapping hysteresis cannot be investigated. In this manuscript use the quasi-static model and focus on the effect of pore geometry on trapping.

[29] Details of the complete algorithm used in this pore-network model have been reported in *Joekar-Niasar et al*. [2008]. Using this model, we are able to track trapped regions of the nonwetting phase in any sequence of drainage and imbibition scanning curves in a completely water-wet system.

[30] As shown in Figure 4, the pore network is made of large pores, referred to as pore bodies, connected to each other through small (narrow) pore throats. Sizes of pore bodies follow an uncorrelated truncated log-normal distribution and sizes of pore throats are determined based on the neighboring pore bodies. Mean, minimum, maximum and standard deviation of pore bodies are 0.108, 0.055, 0.3, and 0.04 mm, respectively.

[31] *Joekar-Niasar et al*. [2010b] have discussed the significant effect of angularity of pore elements on calculated residual wetting phase, entry capillary pressure, and two-phase conductance. To incorporate a measure of angularity and irregularity of the solid surfaces (which is typical of natural porous media), we have assigned different polygonal cross sections in addition to circular cross sections. The pore throats can have circular or *n*-edged regular polygonal cross sections. The number of edges, *n*, is an input parameter. The pore bodies have been represented by spheres or cubes. The shape of pore throat cross sections and pore bodies control the amount of residual saturation at the pore level and consequently at the representative elementary volume (REV) scale. Major pore-scale invasion mechanisms such as piston-like movement, snap off, and cooperative pore filling have been included. We refer to *Joekar-Niasar et al*. [2010a] for further information. For an imposed capillary pressure under equilibrium conditions, the occupancy of pore throats and pore bodies, during imbibition or drainage, has to be determined. To obtain the fluid occupancy, an entry capillary pressure for a pore throat for a given geometry is calculated [*Joekar-Niasar et al*., 2010a], which depends on pore geometry, interfacial tension and contact angle. Here, we use the interfacial tension for air-water equal to 0.0725 N/m and the contact angle equal to 4°.

[32] When the pore elements have angularity, there is always a residual wetting phase in the corners, controlled by the capillary pressure. The radius of a capillary interface in each pore will change with the global capillary pressure (if the nonwetting phase is connected to its reservoir) and consequently, the wetting phase saturation as well as the two-phase conductance will change, even when no piston displacement takes place.

[33] Under imbibition condition, with decrease of the nonwetting phase pressure, the capillary interfaces start to relax. Since the pore throats are smaller than the pore bodies the critical capillary pressure at which the capillary interface would no longer be stable is higher than that of pore bodies. As soon as the external pressure difference is smaller than the critical snap off capillary pressure for a pore throat, the pore throat will be filled by the wetting phase. To identify whether the local snap off in a pore throat makes creation of a trapped nonwetting ganglia, a search algorithm is done at each pressure step to identify where the nonwetting phase has been disconnected from its corresponding boundary. At the end of each search step the nonwetting phase at each pore element is flagged as disconnected or connected.

[34] Saturation of each phase is calculated as the total volume of each phase (in pore bodies and throats) divided by the total void volume. Knowledge of the fluid occupancy of pore bodies and pore throats allows the connected and disconnected fluids at each pore to be identified using a search algorithm. Because the wetting phase is assumed always to be connected to its corresponding reservoir, there is no disconnected wetting phase.

[35] To calculate the relative permeability, first the network of continuous pathways is identified. The continuous pathway is identified by a search algorithm starting from one reservoir boundary and tracking across the network to the other reservoir boundary. If a fluid does not have a continuous path across the network, its permeability is set to zero. We calculate the phase conductance in each pore for the given capillary pressure following *Patzek* [2001].

[36] Given the conductance of phase α in a pore throat ij (denoted by K_{ij}^{α}), the Hagen-Poiseuille equation can be used to relate the flux, Q_{ij}^{α}, to the phase pressure drop Δp_{ij}^{α} by $Q_{ij}^{\alpha} = K_{ij}^{\alpha} \Delta p_{ij}^{\alpha}$. For the pressure field an assigned pressure difference across the network (Δp^{α}) is obtained from the volumetric conservation law for each pore body. This conservation law is a linear set of equations given by

$$\sum_{j=1}^{n_i} Q_{ij}^{\alpha} = \sum_{j=1}^{n_i} K_{ij}^{\alpha} \Delta p_{ij}^{\alpha} = 0, \qquad i = 1, 2, \ldots, N_p \tag{14}$$

where n_i is the number of pore throats connected to the pore body i and N_p is the total number of pore bodies

[37] After solving the equation system for the pressures field, the inflow rate $\left(Q_{in}^{\alpha}\right)$ can be calculated. Phase permeability at a given saturation is given by

$$K^{\alpha}(S_w) = \frac{\mu^{\alpha} Q_{in}^{\alpha} L}{A \Delta p^{\alpha}} \tag{15}$$

where L and A denote the length and cross sectional area of the network, and μ^{α} denotes the viscosity of phase α. The relative permeability will be $k_r^{\alpha} = K^{\alpha}/K$ in which K is the intrinsic permeability of the network. The intrinsic permeability is calculated in the same fashion for a fully saturated system.

[38] Finally, note that to be able to present results that can be applied to continuum-scale models discussed in the previous section, the network size should be chosen so that at least an REV size is satisfied. For the given statistical properties (pore body and pore throat sizes) the results were independent of the network size for networks larger than a cubic network with 25 pores in each dimension. As such we used a network with 25 pores in each direction.

4. Results and Discussion

[39] Here, we will compare the trends of the simulation results with the trapping models. Effects of pore-scale mechanisms on trapping during drainage and imbibition and on constitutive relations at the REV scale will also be presented and discussed.

4.1. Analysis of Trapping Models Based on the Pore-Network Results

[40] Based on the simulation results, it is possible to examine the agreement between our results and the proposed trapping models in the literature. Primary and main drainage, main imbibition, and several scanning drainage and imbibition curves have been simulated. Examples of drainage-imbibition-drainage sequence are given in Figures 5a and 5b. Note that drainage and imbibition curves have been generated for various turning points.

[41] Both figures show that the relationship between trapped nonwetting-phase saturation and total wetting phase saturation is hysteretic, consistent with *van Kats and van Duijn* [2001] and *Hilfer* [2006]. For a given wetting-phase saturation, disconnected nonwetting-phase saturation is larger during drainage than during imbibition. This requires $\eta < 1$, while the model from *Hilfer* [2006] requires $\eta > 1$ to obtain capillary pressure saturation relationships

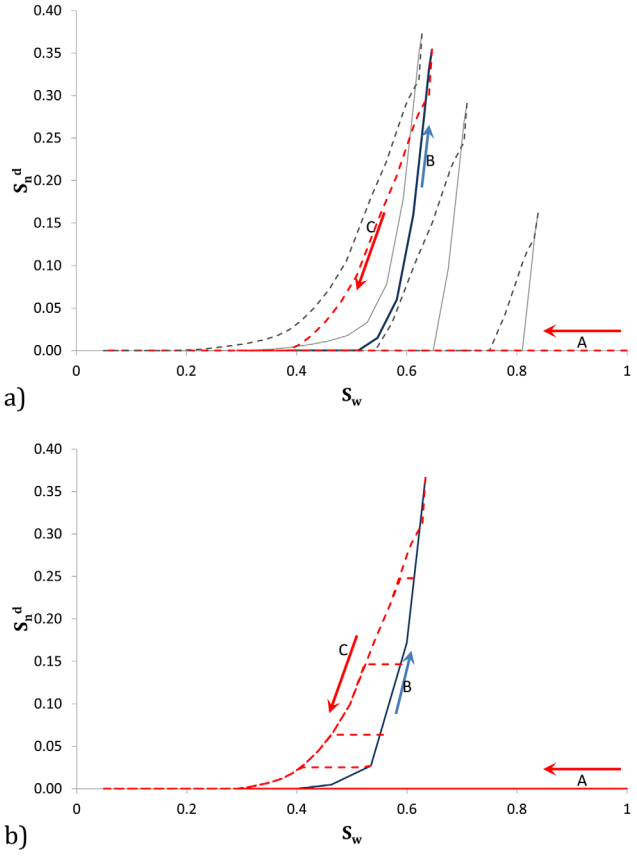

Figure 5. Disconnected nonwetting-phase saturation versus wetting phase saturation for primary drainage followed by different imbibition(solid)-drainage(dashed) loops. (a) The loops are started at different turning saturations S_n^t and the imbibition is completed so that only disconnected nonwetting phase remains at the end of the imibibiton process. (b) All loops start at the same turning saturation but the secondary drainage is started at various saturations before the imbibition process is completed. The sequence of the simulations is A→B→C. Pore throats have square cross sections and pore bodies are cubic.

that agree with experimental observations. The trend of S_n^d-S_w curve can also be examined based on the pore-scale insights of two-phase flow. The maximum rate of production of disconnected nonwetting phase versus total wetting phase saturation $\left(\partial S_n^d / \partial S_w\right)$ occurs close to the end of the imbibition curve (Figure 5a). When S_w is very small, the nonwetting phase can be connected by several flow paths to its boundary. However, at large S_w the nonwetting phase loses its connections to the boundary. At a later stage of imbibition, a single path can be critical as it may be the only path the connects a nonwetting fluid cluster to the nonwetting phase reservoir. If this connection is lost, all remaining nonwetting phase will be trapped. Moreover, our results show an obvious dependence of the residual saturation on the turning saturation (Figure 6 and the discussion below).

[42] The general trend observed during imbibition is qualitatively in agreement with the trapping models suggested by *Land* [1968], *Lenhard et al.* [1991], and *Jerauld* [1997]. Comparing the results with the models proposed by

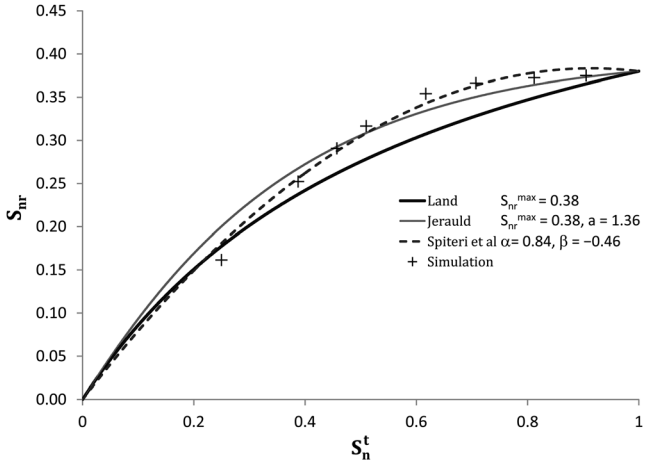

Figure 6. Residual saturation versus turning saturation for a network with square cross-sectional pore throats.

Parker et al. [1987] and *Lenhard and Parker* [1987] we see that a linear interpolation between turning saturation and residual saturation is not a good model.

[43] In contrast to the drainage curves in Figure 5a, where the initial $S_n^c = 0$, in Figure 5b the secondary drainage starts while there is still connected nonwetting phase left, $S_n^c \neq 0$. The comparison between the drainage curves started from $S_{nr}(S_n)$ (the most outer loop in Figure 5b and all loops in Figure 5a) and the drainage curves started before S_{nr} (the four internal loops in Figure 5b) suggests that trapping during drainage is significantly influenced by the nonwetting fluid topology at the start of a drainage path. In an angular network at the start of a drainage path, if $S_n^d \neq S_{nr}$, the trapped nonwetting phase saturation remains unchanged while the wetting-phase saturation changes. The extension of this trend depends on the angularity of the medium and will be discussed in detail in the next section.

[44] We note that, although *Spiteri et al*. [2005] also used pore-network modeling to analyze hysteresis in relative permeability, they did not report this kind of behavior. They did not focus on the scanning (especially drainage) curves nor on the effect that pore geometry has on trapping and consequently on relative permeability curves.

[45] Another important issue that has been addressed by trapping models is that the final value of the trapped nonwetting-phase saturation depends on the turning point saturation. This dependence is shown in Figure 6 based on the pore-network results. Models proposed by *Land* [1968], *Lenhard et al*. [1991], *Jerauld* [1997], and *Spiteri et al*. [2005] have been fitted to the data as well. The results show that for a large value of the turning-point saturation, S_n^t, the residual saturation $S_{nr}(S_n^t)$ displays a weak dependence on S_n^t. All fits approximate the relation reasonably well. The best fit is obtained by the relation of *Spiteri et al.* [2005].

4.2. Reversible Corner Filling Mechanism and Trapping

[46] As shown in Figure 5b, the initial topology of the nonwetting fluid during drainage can influence the trajectory of S_n^d versus S_w. Specifically, S_n^d can remain constant as S_w is decreasing. This behavior can be explained by considering the cross-sectional configurations of pores filled with both fluids (inset in Figure 4). Consider a snapshot of fluids where there is still nonwetting phase connected to the nonwetting phase reservoir, as the initial condition for a drainage event. Next to the nonwetting phase, there might be some pores that are only filled with the wetting phase. To drain those pores, global capillary pressure should exceed the entry capillary pressure of these pores. If the pressure increase is smaller than the entry capillary pressure, the fluids topology does not change.

[47] However, the nonwetting fluid will invade into the corners of already filled pores, thereby allowing both S_n and S_w to change (but not S_n^d). We refer to this mechanism as "reversible corner filling." As a result, the wetting-phase saturation will decrease, the nonwetting-phase saturation will increase but the disconnected nonwetting phase saturation will remain unchanged. As long as the fluid topology does not change, this process is reversible. This "reversible cornering filling" mechanism is also valid when there is hysteresis in contact angle. *Braun and Holland* [1995] investigated the reversibility of the relative permeability curves in porous media with hysteretic contact angle. Based on their experimental observations, they proposed the "pinning mechanism" and stated that "as long as the interfaces remain pinned (in the corners), changes in fluid geometry are reversible. Outside the range of reversibility, contact angles are at their limiting values, interfaces move along grain surfaces, and fluid geometries are controlled by processes that result in hysteresis." The mechanism we identify is analogous to this kind of pinning, although there is no common line in our case. We conjecture that as long as the fluid topology does not change, the motion of the interface remains reversible.

[48] The relationship between trapped nonwetting-phase and wetting-phase saturation depends on the pore geometry, fluid topology, and contact angle hysteresis. The "reversible corner filling" depends significantly on the angularity of the domain and the initial nonwetting fluid topology. Figure 7a shows the variation of the disconnected nonwetting-phase saturation versus total wetting phase saturation for three networks with the same topology but different pore cross sections: (1) triangular pore throats with cubic pore bodies, (2) parallelepiped pore throats with cubic pore bodies, and (3) cylindrical pore throats with spherical pore bodies. The figure shows a primary drainage followed by an imbibition followed by another drainage for each of the three networks. In circular cross sections, the trend of S_n^d versus S_w during drainage is independent of initial nonwetting fluid topology, while in triangular cross sections, S_n^d remains constant for a large range of S_w. This is explained by the amount of the wetting phase that can accumulate in the corners, that is, the difference between the areas of the cross section and the inscribed circle in pore throats or the difference between the volumes of pore bodies and the inscribed spheres. Coupled with the experimental observations, these results strongly argue for the reversible corner filling mechanism.

[49] Figure 7b illustrates the impact of pore aspect ratio (ratio of pore body to pore throat radii) as well as hysteresis of advancing and receding contact angle on trapping of the nonwetting phase. The figure shows that for an increased receding contact angle (from 0 to 20°), the capillary

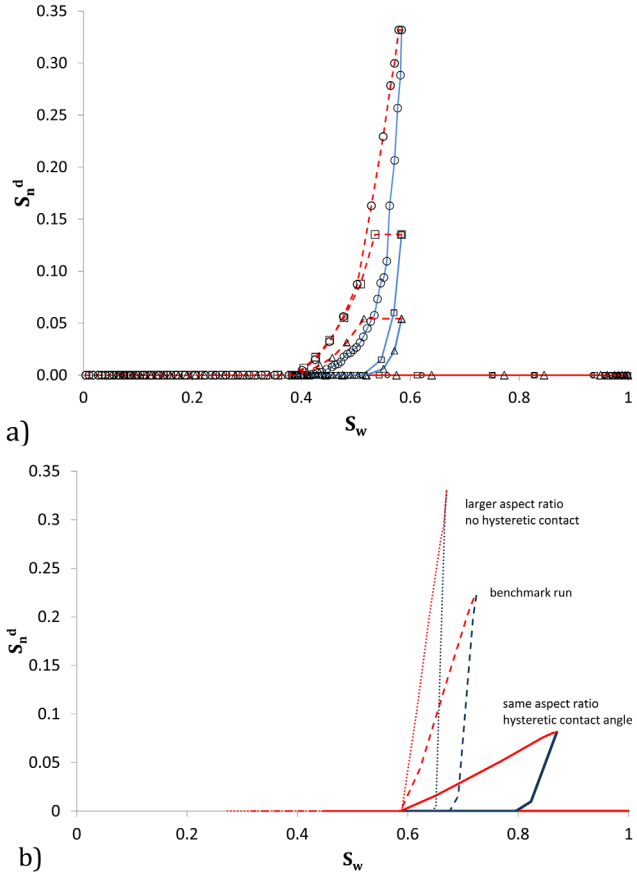

Figure 7. (a) Effect of pore geometry on S_n^d-S_w curve under drainage for circular (shown by circle), parallelepiped (shown by square), and triangular (shown by triangle) pore throats. Drainage and imbibition curves have been shown in red and blue, respectively. (b) Effect of contact angle hysteresis and pore aspect ratio on capillary trapping. In the hysteretic contact angle, receding contact angle has been set to 20° and advancing to 0.

trapping of the nonwetting phase decreases significantly, while the capillary pressure curves (not shown here) do not change as much. Our pore-network model results show that the effect of contact angle hysteresis on relative permeability hysteresis is stronger than on the capillary pressure hysteresis. However, since this is not the main focus of the paper, these results are not shown in the manuscript.

[50] The pore aspect ratio determines the snap off under capillary dominated imbibition. We have kept the pore bodies the same as the benchmark run but have taken smaller pore throat radii. We changed the aspect ratio by approximately 20%. The contribution of the pore throats to the pore volume is small, and therefore this does not alter porosity significantly. However, the increased aspect ratio has a significant effect on the early trapping of the nonwetting phase under imbibition. As a consequence, both the capillary pressure curve and the relative permeability curves show a significant increase of hysteresis (results not shown here). Thus, the simulation results imply that the sensitivity of the macroscopic constitutive relations as well as the trapping relations to the aspect ratio is more than that to the contact angle hysteresis in water wet systems.

4.3. Comparison to Laboratory Experiments

[51] To support the simulation results, specifically the reversible corner filling trapping mechanisms, we examined a particular set of experimental data measured on a volcanic tuff material (the manuscript for this experimental work is in preparation). A brief description of the experiments is provided here, for more general details we refer to *Porter et al*. [2010].

[52] In these experiments, a number of air-water drainage and imbibition cycles were completed on a 6 mm inner diameter sample of crushed volcanic tuff. The granular material consisted of quartz, feldspar, and albite, and had a D50 (called the median grain size is the grain diameter for which half the sample (by weight) is smaller and half is larger) of 1795 μm. The scheme of the experimental setup is shown in Figure 8. A precision syringe pump was used to imbibe and drain water to and from the sample, a semipermeable membrane was used below the sample to prevent air from entering the pump line, and the air phase was at atmospheric pressure on top.

[53] The experiment was started with a dry sample and the sample was taken through primary imbibition and drainage cycles. Imaging (and saturation measurement) started with the first imbibition cycle (performed at 1 mL/h). All the experiments were performed consecutively, such that the end point of each imbibition cycle comprised the first point on the subsequent drainage cycle, and so on.

[54] The sample was allowed to equilibrate for 10 min before it was imaged, and imaging took approximately 10 min. No blurring was observed during imaging, which indicates that no interfaces were moving during the 10 min scan; however, that does not preclude longer term equilibration, and as such we can only assume that the sample was in a pseudoequilibrium state. During the drainage and imbibition cycles, fluid saturations and distributions were measured using X-ray computed microtomography at the GeoSoilEnviroConsortium for Advanced Radiation Sources beam-line 13-BMD at Argonne National Lab. The water phase was spiked with potassium iodide (1:6 weight ratio of KI to water) to enhance contrast in the images. An energy level just above the iodine photoelectric edge (33.22 keV) was used for imaging. The gray-scale data was segmented using the approach described in *Porter and Wildenschild* [2010]. The resulting image volumes were cropped for final analysis to a cube with dimensions of 294 × 294 × 378 voxels, with a voxel resolution of 16.8 μm, this comprises a cube of 4.9 mm × 4.9 mm × 6.4 mm = 154.9 mm^3.

[55] The nonwetting phase that occupies this pore space was then separated into connected and disconnected phases using an algorithm in Avizo Fire® called "Reconstruct." A nonwetting phase marker was placed at the top region of the analyzed pore space (i.e., the region from which nonwetting phase retreats during imbibition), and any nonwetting phase voxel not connected to this marker was considered disconnected. Using this approach the imaged volume was segregated into connected and disconnected nonwetting phase. Lastly, connected and disconnected phase saturations were calculated by voxel counting.

[56] A full closed cycle of drainage and imbibition (for S_n^d versus S_w) is shown in Figure 9a. The experiments are

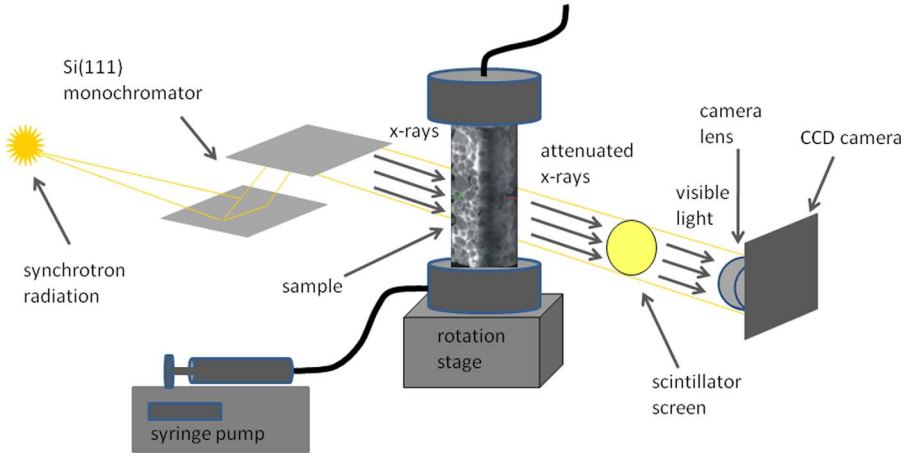

Figure 8. Schematic presentation of the experimental setup.

consistent with the simulations in that, under drainage, there is more disconnected nonwetting phase, compared to imbibition, for a given saturation. Interestingly, during the main drainage measurements, S_n^d did not change significantly with S_w at high saturations, which is consistent with the reversible corner filling mechanism. To be even more precise, we visualized fluid distributions in a part of the medium to show why this plateau was observed. The images shown in Figure 9b were selected such that they represent similar disconnected saturations but with different wetting saturations. The images show that, while nonwetting phase invades the sample (violet) and S_w changes significantly, the disconnected nonwetting phase remains almost constant. These observations are consistent with the physical mechanisms captured in the pore-network model as the underlying process of capillary trapping and the plateau in S_n^d-S_w. As additional corroboration, we note that "reversible corner filling" was not observed in glass bead experiments using the same fluids (results not presented here).

4.4. Effect of Trapping on Constitutive Relationships

[57] Figures 10a–10d show the simulation results for a network with parallelepiped pore throats and cubic pore bodies. Several continuous drainage and imbibition simulations have been performed. As Figure 10a shows there is no disconnected nonwetting phase under primary drainage (from points 1 to 2). In the first scanning imbibition curve (points 2 to 3) the nonwetting phase eventually becomes disconnected. The subsequent drainage scanning curve (points 3 to 4) shows no plateau behavior (Figure 10a) and therefore no corner filling mechanism. The next imbibition cycle (points 4 to 5) stops (point 5) before all of the nonwetting phase is disconnected. The following drainage curve (points 5 to 6) shows a pronounced plateau region, driven by the reversible corner filling mechanism. Similar behavior is seen through the subsequent scanning cycles, until the ending point (point 9).

[58] Looking at Figure 10b, we can see the influence of nonwetting-phase connectivity on macroscopic P_c-S_w curves. Drainage scanning curves that begin with all nonwetting fluid being trapped (for example, beginning at point 3) show the usual shape that is concave downward (that is, the curvature is negative, $d^2P_c/dS_w^2 < 0$). However, when some connected nonwetting fluid is present at the onset of the next drainage cycle (points 5 and 7), the corner filling mechanism is important, and the shape of the resulting drainage scanning curve changes qualitatively so that the curve is concave upward $\left(d^2P_c/dS_w^2 < 0\right)$. We are unaware of any other reports of such behavior, although the experimental results of *Chen et al*. [2007] appear to show somewhat similar behavior. As a remark, with introducing hysteresis in the contact angle there would be some differences in shapes of scanning capillary pressure curves under drainage and imbibition. The imbibition scanning curves do not show any similar changes. The implications of this behavior in the drainage scanning curves remain to be explored. We observe that simple scaling of the main drainage curve to define the scanning curves would appear to be inappropriate for these cases.

[59] Finally, the effect of nonwetting-phase connectivity on relative permeability curves is shown for the same set of simulations. As the wetting phase is assumed to be always connected to its reservoir, there is no significant difference between drainage and imbibition wetting-phase relative permeabilities (Figure 10c). However, nonwetting-phase relative permeabilities show a significant hysteresis (Figure 10d) driven mainly by the corner filling mechanism. This behavior has also been reported in *Jerauld and Salter* [1990, Figure 13], where a larger nonwetting phase relative permeability under imbibition compared to drainage is observed (for a water wet system). Note that these results differ from those of *Spiteri et al*. [2005]. In their work, they assumed that all hysteresis in relative permeability curves can be removed, if they are plotted against the connected saturation instead of total saturation. However, our results show that although the hysteresis will be reduced, there will still be a difference between relative permeability curves under drainage and imbibition due to the "reversible corner filling" mechanism.

[60] As mentioned before, no dynamic effects have been incorporated in the simulations. Thus, once a region of disconnected nonwetting phase is created, it will be static and will not mobilized. Under dynamic conditions, it is possible

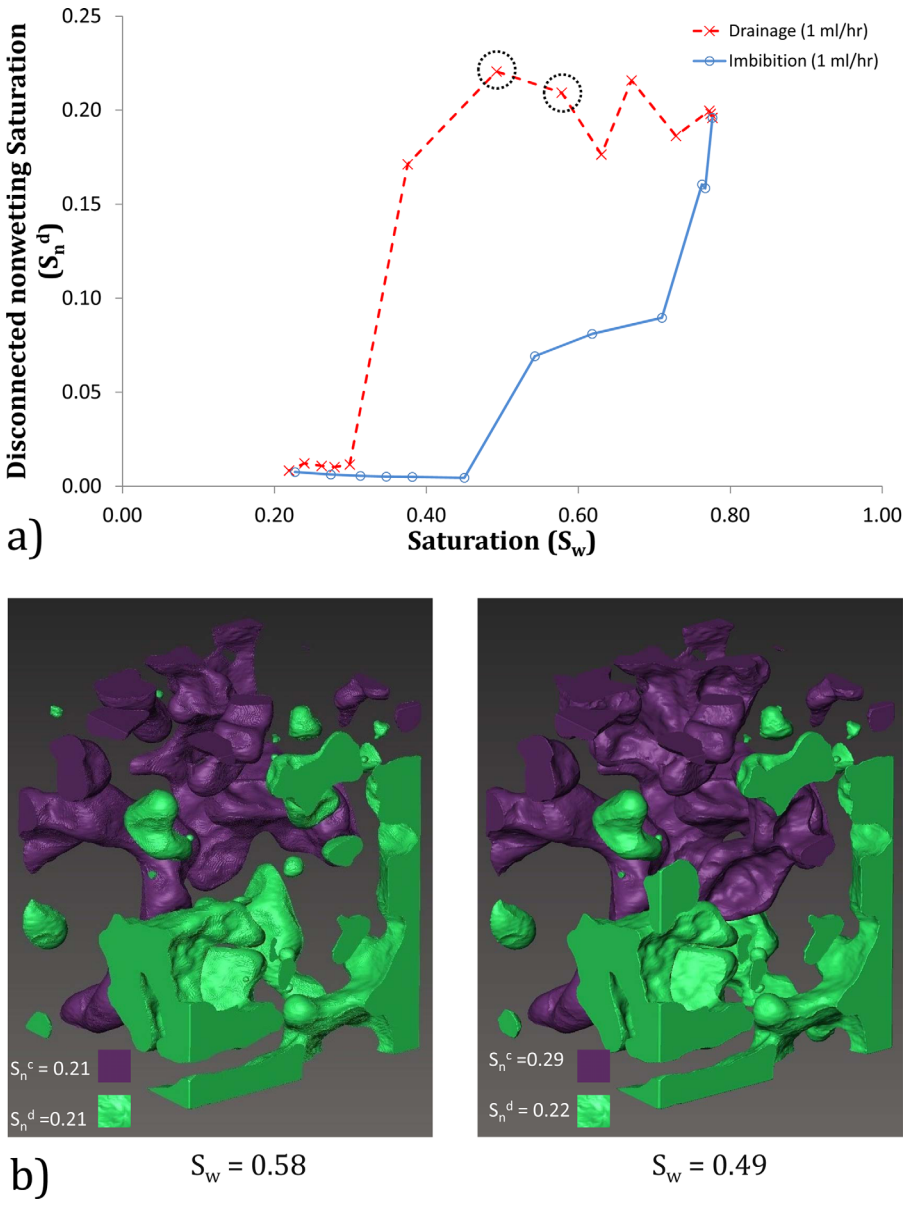

Figure 9. (a) Variation of disconnected nonwetting phase saturation S_n^d versus wetting phase saturation S_w for main drainage (red/dashed line) and imbibition (blue/solid line) experiments in volcanic tuff. (b) A part of the sample at two drainage observation points has been visualized to illustrate the "reversible corner filling" mechanism. The violet color represents the connected nonwetting phase, and the green color represents the disconnected nonwetting phase.

to mobilize the capillary trapped ganglia by viscous forces or by reduction of capillary forces. We plan to study dynamic effects on trapping in a later publication.

5. Summary and Conclusion

[61] We have used a quasi-static pore-network model to show the underlying mechanisms that influence trapping of the nonwetting phase as a function of wetting phase saturation. Results of the pore-network model have been related to proposed trapping models in the literature and have provided new insights into the physics of the problem.

[62] All results show a strong hysteresis in trapping during drainage and imbibition, which is in agreement with trapping models suggested by *van Kats and van Duijn* [2001] and *Hilfer* [2006]. However, the trend of disconnected nonwetting-phase saturation versus total wetting-phase saturation shown in the simulations and pore-scale visualizations is in disagreement with the proposed trend by *Hilfer* [2006]. Interestingly, trapping during drainage shows a strong dependence on nonwetting-phase fluid topology was well as pore geometries including angularity and aspect ratio. If the nonwetting phase is connected to its boundary at the onset of the drainage cycle, with gradual change of capillary pressure, total phase saturation will also change while the disconnected nonwetting phase may not change. This mechanism, which is referred to as "reversible corner filling," has not been incorporated into any

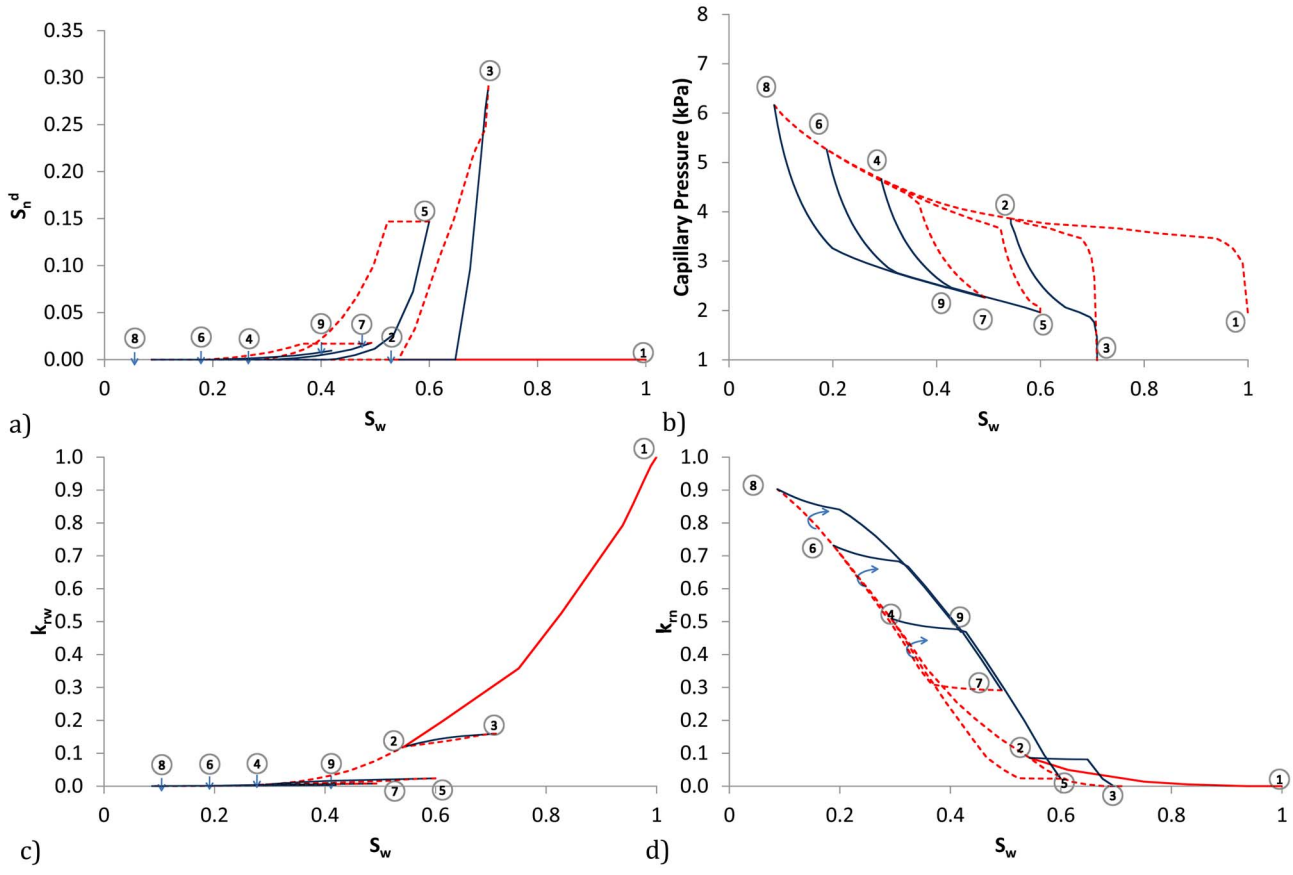

Figure 10. Pore-network simulation results for parallelepiped pore throats and cubic pore bodies showing the variation of (a) S_n^d versus S^w (b) P^c versus S^w (c) k_{rw} versus S^w, and (d) k_{rn} versus S^w for several drainage and imbibition cycles. The turning points have been numbered sequentially. Drainage and imbibition trajectories have been shown in red and blue, respectively.

existing trapping model. This mechanism was also observed in laboratory experiments performed in a volcanic tuff where the pore geometry is very irregular. But, it was not observed in two-phase experiments in glass beads where the pore geometry is very smooth and connected corner flow is not expected to occur. These observations are all consistent and point to reversible corner filling as a potentially important mechanism.

[63] The contribution of nonwetting fluid topology and pore geometry to relative permeability-saturation and capillary pressure-saturation curves can be significant. Based on our results, the shape of drainage scanning curves for the capillary pressure can significantly change, if corner flow is significant in a porous medium. This is due to the existence of connected nonwetting phase at the onset of the drainage scanning cycle. Moreover, the wetting phase does not show a strong hysteresis in relative permeability compared to the nonwetting phase, as the topology of the wetting phase does not change significantly with change of saturation. But, the nonwetting phase permeability changes significantly with trapping as its topology changes dramatically. In contrary to *Braun and Holland* [1995], who stated that reversibility of drainage and imbibition requires "pinned contact lines" to the solid surface, "irreversible corner filling" mechanism suggests that as long as the fluid topology does not change while the saturation is changing the displacement process is reversible, without involving contact lines.

[64] Based on our results, existing trapping models will require further development to include effects of porous medium geometry as well as fluid topology. These factors can lead to strong hysteresis and nonlinearities in trapping curves that should be included in the models. Furthermore, the effect of dynamic parameters (such as capillary number and fluids viscosity ratios) on trapping has not been included here but should be studied to develop a more complete picture of trapping and hysteresis.

[65] **Acknowledgments.** This research was funded by Utrecht University (grant KUK-C1–017-12) and in part by the National Science Foundation under grant EAR-0934722.

References

Blunt, M. J. (2001), Flow in porous media—Pore-network models and multiphase flow, *Curr. Opinion Colloid Interface Sci.*, *6*(3), 197–207.

Braun, E., and R. Holland (1995), Relative permeability hysteresis: Laboratory measurements and a conceptual model, *SPE Reservoir Eng.*, *10*(3), 222–228.

Chen, L., G. A. Miller, and T. C. G. Kibbey (2007), Rapid pseudo-static measurement of hysteretic capillary pressure-saturation relationships in unconsolidated porous media, *Geotech. Test. J.*, *30*, GTJ100850, 474–483.

Doster, F., and R. Hilfer (2011), Generalized Buckley-Leverett theory for two phase flow in porous media, *New J. Phys.*, *11*, 123030, doi:10.1088/1367–2630/13/12/123030.

Doster, F., P. A. Zegeling, and R. Hilfer (2010), Numerical solutions of a generalized theory for macroscopic capillarity, *Phys. Rev. E*, *81*(3), 036307, doi:10.1103/PhysRevE.81.036307.

Everett, D. H., and W. I. Whitton (1952), A general approach to hysteresis, *Trans. Faraday Soc.*, *48*(8), 749–757.

Hassanizadeh, S. M., and W. G. Gray (1993), Thermodynamic basis of capillary pressure in porous media, *Water Resour. Res.*, *29*(10), 3389–3405.

Hilfer, R. (2006), Capillary pressure, hysteresis and residual saturation in porous media, *Phys. A*, *359*, 119–128.

Hilfer, R., and F. Doster (2010), Percolation as a basic concept for macroscopic capillarity, *Transp. Porous Media*, *82*(3), 507–519.

Jerauld, G. R. (1997), General three-phase relative permeability model for prudhoe bay, *SPE Reservoir Eval. Eng.*, *12*, 255–263.

Jerauld, G. R., and S. J. Salter (1990), The effect of pore-structure on hysteresis in relative permeability and capillary pressure: Pore-level modeling, *Transp. Porous Media*, *5*, 103–151, doi:10.1007/BF00144600.

Joekar-Niasar, V., and S. M. Hassanizadeh (2011), Specific interfacial area; the missing state variable in two-phase flow?, *Water Resour. Res.*, *47*, W05513, doi:10.1029/2010WR009291.

Joekar-Niasar, V., and S. M. Hassanizadeh (2012), Analysis of fundamentals of two-phase flow in porous media using dynamic pore-network models; a review, *Crit. Rev. Environ. Sci. Technol.*, *42*, 1895–1976.

Joekar-Niasar, V., S. M. Hassanizadeh, and A. Leijnse (2008), Insights into the relationships among capillary pressure, saturation, interfacial area and relative permeability using pore-network modeling, *Transp. Porous Media*, *74*(2), 201–219.

Joekar-Niasar, V., S. M. Hassanizadeh, and H. K. Dahle (2010a), Non-equilibrium effects in capillarity and interfacial area in two-phase flow: Dynamic pore-network modeling, *J. Fluid Mech.*, *655*, 38–71.

Joekar-Niasar, V., M. Prodanović, D. Wildenschild, and S. M. Hassanizadeh (2010b), Network model investigation of interfacial area, capillary pressure and saturation relationships in granular porous media, *Water Resour. Res.*, *46*, W06526, doi:10.1029/2009WR008585.

Land, C. S. (1968), Calculation of imbibition relative permeability for two- and three phase flow from rock properties, *Trans. Am. Inst. Min. Metall. Pet. Eng.*, *243*, 149–156.

Lenhard, R., J. Parker, and J. Kaluarachchi (1991), Comparing simulated and experimental hysteretic two-phase transient fluid flow phenomena, *Water Resour. Res.*, *27*(8), 2113–2124.

Lenhard, R. J., and J. C. Parker (1987), A model for hysteretic constitutive relations governing multiphase flow: 2. Permeability-saturation relations, *Water Resour. Res.*, *23*(12), 2197–2206.

Mualem, Y. (1974), A conceptual model of hysteresis, *Water Resour. Res.*, *10*(3), 514–520.

Niessner, J., and S. M. Hassanizadeh (2008), A model for two-phase flow in porous media including fluid-fluid interfacial area, *Water Resour. Res.*, *44*(8), W08439, doi:10.1029/2007WR006721.

Parker, J. C., and R. J. Lenhard (1987), A model for hysteretic constitutive relations governing multiphase flow: 1. Saturation pressure relations, *Water Resour. Res.*, *23*(4), 618–624.

Parker, J. C., R. J. Lenhard, and T. Kuppusamy (1987), A parametric model for constitutive properties governing multiphase flow in porous media, *Water Resour. Res.*, *23*(4), 618–624.

Patzek, T. W. (2001), Verification of a complete pore network simulator of drainage and imbibition, *SPE J.*, *6*, 144–156.

Porter, M., and D. Wildenschild (2010), Image analysis algorithms for estimating porous media multiphase flow variables from computed microtomography data: A validation study, *Comput. Geosci.*, *14*, 15–30.

Porter, M. L., D. Wildenschild, G. Grant, and J. Gerhard (2010), Measurement and prediction of the relationship between capillary pressure, saturation, and interfacial area in a napl-water-glass bead system, *Water Resour. Res.*, *46*, W08512, doi:10.1029/2009WR007786.

Scott, P. S., G. J. Farquhar, and N. Kouwen (1983), Hysteretic effects on net infiltration, *Am. Soc. Agric. Eng.*, *11-83*, 163–171.

Spiteri, E. J., R. Juanes, M. J. Blunt, and F. M. Orr Jr. (2005), Relative permeability hysteresis: Trapping models and application to geological CO2 sequestration, paper presented at SPE Annual Technical Conference and Exhibition, Dallas, Tex.

van Kats, F., and C. van Duijn (2001), A mathematical model for hysteric two phase flow in porous media, *Transp. Porous Media*, *43*, 239–263.